




Electron-Beam Reflection Investigation Concerning Charged Disc and Multipole Approximations

Tareq H. Abbood¹, Hassan N. Al-Obaidi^{1*}, Ali S. Mahdi², Wasan J. Kadhem³, Faten H. Mousa²

¹ Department of Physics, College of Education, Mustansiriyah University, Baghdad 10052, Iraq

² Ministry of Education, Open-Education College, Baghdad 10053, Iraq

³ Department of Scientific Basic Sciences, Faculty of Engineering Technology, Al-Balqa Applied University, Amman 19117, Jordan

Corresponding Author Email: hassannouri@uomustansiriyah.edu.iq

Copyright: ©2024 The authors. This article is published by IIETA and is licensed under the CC BY 4.0 license (<http://creativecommons.org/licenses/by/4.0/>).

<https://doi.org/10.18280/mmep.110810>

ABSTRACT

Received: 13 April 2024

Revised: 20 June 2024

Accepted: 28 June 2024

Available online: 28 August 2024

Keywords:

mirror effect, scanning electron microscope, electron beam, insulating materials and surface potential

The influence of the surface sample potential on the head-incident electron beam in the scanning electron microscope has been studied in terms of the mirror effect. The multipole and charged disc models have been used to approximate the sample potential. The energy conservation law is used to assist set up the equation of motion for the incident electron. The point of reflection of the electrons along the length between the sample surface and the column diaphragm is then determined by solving the equation. In fact, the beam and surface potential characteristics mostly determine the reflection point's value. In light of the variations between the two models that were utilized, the reflection behavior was examined in terms of these characteristics. The outcomes have demonstrated that, when it comes to simulating the surface potential, each model has both advantages and disadvantages. In reality, the two models exhibit comparable results over a broad range of distances between the sample surface and the column diaphragm when the common parameters are placed in parallel. However, the variance between them occurs in a very short distance that almost does not exceed 13% approximately. Nevertheless, because of its own mathematical nature, the multipole model is best appropriate to estimate the surface potential of highly concentrated trapped charges. Meanwhile, the charged disc model is suitable for approximating the surface potential for low concentrated trapped charges.

1. INTRODUCTION

Material examination by means of charged particle devices, especially the scanning electron microscope (SEM) and focused ion beam (FIB), differ according to the sort of material, whether it is an insulator or conductor. Insulator inspections are generally associated with an undesirable problem compared to conductors, due to their ability to trap the electron for a period. The accumulation of electrons on the surface of the insulating sample continues as long as the irradiation process persists. Gradually, these electrons form a layer with an area and a width that depends on the energy of the irradiation beam [1], the time of irradiation [2, 3], and the characteristics of the insulator itself [4]. Such a layer leads to generating an electric potential, which causes the next incoming electrons to reflect and prevents them from reaching the sample. However, the reflected electrons interact with the upper parts of the space chamber and thus the image of the appearance for these parts instead of the sample surface. Images obtained in this manner are called electron mirror images (EMI) and the phenomenon leads to generating these images, usually named as mirror effects (ME) or charging effects (CE).

Reasonably, the reflection behavior of incident electrons depends primarily on the form of the electrical potential characteristics generated by the trapped electrons. Many authors have discussed this issue, but the actual distribution of such potential throughout the chamber space is far from well-defined. A number of models have been proposed to simulate this superficial potential concerning the distribution of the potential and the profile in which the trapped electrons accumulated. For example, the charged-point model (or point charge model as it is named sometimes) is widely adopted, especially when (EMIs) are captured by low scanning potentials [5-8]. At the time when there is almost a single form for the charged-point model, the charged-disc model has several representations. However, the basic form of this model is used to prove some aspects [3, 9, 10]. Meanwhile, a modified form of such a model is adopted to meet some advanced tasks [11]. In fact, the multipole model is the most efficient model for investigations due to its ability to simulate EMI that is captured by a wide range of scanning potential. Indeed, this approximation also has a variety of mathematical representations based on different assumptions [12-17].

Absolutely, EMI properties depend not only on the surface potential, but also on the characteristics of the incident beam

of electrons. Therefore, the characteristics of an EMI are a result of the interaction of the electron beam with the surface potential. Such interaction has already been investigated in terms of a charged disk model that is used to approximate beam and surface potentials [9, 10]. Actually, the charged disk model is useful in certain circumstances, but it is not the optimal approximation of the surface potential. Therefore, the aspect of interaction between the beam and the sample potentials is far from obvious and deserves a closer look. It is thus entirely appropriate to explore another model to analyze such an interaction in the sense of EM. Consequently, the present work has proposed to adopt one of the most interesting forms of the multipolar model in order to investigate the beam-sample interaction.

The multipolar model has been selected as the "target function" for the current investigation for two reasons. The first is that a wide range of realistic distributing profiles where the trapped electrons could occur are covered by this model [16]. For the second reason, however, the multipolar model shows that the trapped electrons can organize into many configurations, such as octupole, quadrupole, dipole, monopole, and so on [17]. Consequently, it is implicitly assumed that the charged-point model is considered in terms of the monopole term when the multipolar model is employed. Hence, the adoption of the multipolar model in the current work implies an indirect implementation of the charged-point model. In a strict sense, the outcomes of the multipolar model involve some of the outcomes of the charged-point model. Therefore, comparing the results of the charged-disk model achieved previously [16, 17] may show the advantages and disadvantages of all of these models.

2. MODELING APPROACH FOR ELECTRON-BEAM REFLECTION

Assuming there is an amount of charges (Q) uniformly distributed in a disc of radius R . Due to this, an electric potential $U(z)$ deduced at a distance r from the center of this disc given by [9]:

$$U(z) = \frac{Q}{2\pi\epsilon_0 R^2} [(z^2 + R^2)^{1/2} - z] \quad (1)$$

Actually, the basic aspects of electromagnetism were used to derive this equation. Furthermore, the disc of electrons is assumed to be at a right angle with respect to the beam axis, see the literature [9] for more details. Anyway, Eq. (1) represent a general form for the charged-disk model in free space where the permittivity is ϵ_0 . Now this formula can successfully carry out to set up the potential of both of the beam and surface potential.

As far as the beam potential is concerned, consider a beam of electrons inside the chamber of a SEM with a radius of R_b and a beam current of I_b . Actually, the electrons that synthesize the beam's face will generate a potential $U_b(z)$ according to Eq. (1), which may be expressed in the following form [18]:

$$U_b(z) = \frac{I_b t}{2\pi\epsilon_0 R_b^2} [(z^2 + R_b^2)^{1/2} - z] \quad (2)$$

Eq. (3) was setup assuming that electrons are distributed uniformly throughout the beam surface. Thus, the face of this

beam being a disc of radius R_b carries electrons of amount $Q_b = I_b T$. The symbol T refer to the time, which elapse when the Q_b electrons pass through any point (x, y, z) within the beam space.

Concerning with surface potential surface, consider a SEM chamber where a sample of material with a dielectric constant ϵ_m needs to be examined. So, when a Q_t of electrons accumulated on the surface of a such material, the produced potential $U_{sd}(z)$ according to Eq. (1) is given by:

$$U_{sd}(z) = \frac{K Q_t}{2\pi\epsilon_0 R_s^2} [(z^2 + R_s^2)^{1/2} - z] \quad (3)$$

Indeed, the radius of the disc where the quantity of trapped electrons Q_t at the material surface is located is indicated by the symbol R_s . The constant K relates the permittivity of the material ϵ_m and that of the free space ϵ_0 through the relative permittivity ($\epsilon_r = \epsilon_m / \epsilon_0$) according to the formula $K = 2 / (\epsilon_r + 1)$. Therefore, the presence of this constant in such an equation refers to the dependence of $U_{sd}(z)$ on the type of the material under consideration. Furthermore, Eq. (3) has derived regarding the optical axis of the SEM column crossing the center of the charged disc vertically. Indeed, it describes the surface potential distribution along the interval that their terminal points are respectively the sample surface and the column diaphragm. In fact, this interval is called the working distance of the SEM (or FIB) apparatus and usually denoted by W .

In addition to the general form of the charged-disk model, another one can be used to approximating the surface potential for the dielectric sample inside the chamber of SEM. Such a form named by multipolar model and represented by the following expression [16]:

$$U_{sm}(r) = \frac{K Q_t}{4\pi\epsilon_0} \left[\frac{1}{\rho} - \frac{3r'}{8\rho^2} + \frac{r'^3}{16\rho^4} \right] \quad (4)$$

When Q_t electrons have accumulated on the sample surface within a spherical region of radius r' , Eq. (4) describes the surface potential that is deduced at the radial point ρ . However, along the distance that separates the sample surface and the column diaphragm, Eq. (4) can be rewritten as follows:

$$U_{sm}(z) = \frac{K Q_t}{4\pi\epsilon_0} \left[\frac{1}{z} - \frac{3r}{8z^2} + \frac{r^3}{16z^4} \right] \quad (5)$$

Now, at the axial point z_r where the incident electrons are reflected back, energy conservation law requires an equal amount of beam and sample potential. Such an equivalence must occur between the potential of the beam and the scanning potential (V_{sc}) on the one hand, and the potential surface on the other hand. As a result, the following two expressions can be setup for the charged disc and multipole models respectively:

$$\frac{K Q_t}{I_b t} \left(\frac{R_b}{R_s} \right)^2 \{ (z_r^2 + R_s^2)^{\frac{1}{2}} - z_r \} - \{ (W - z_r)^2 + R_b^2 \}^{\frac{1}{2}} - (W - z_r) - \frac{2\pi\epsilon_0 R_b^2}{I_b t} V_{sc} = 0 \quad (6)$$

$$\frac{K Q_t}{2 I_b t} R_b^2 \left\{ \frac{1}{z_r} - \frac{3 r'^2}{8 z_r^2} + \frac{1}{16} \frac{r'^3}{z_r^4} \right\} - \{ (W - z_r)^2 + R_b^2 \}^{\frac{1}{2}} - (W - z_r) - \frac{2\pi\epsilon_0 R_b^2}{I_b t} V_{sc} = 0 \quad (7)$$

Therefore, the exploration of the reflection position of an incident electron can be performed using the last two expressions. Actually, this reflection occurs away from the sample surface by a distance z_r or equivalently by a distance $(W-z_r)$ away from the column diaphragm. Surely, z_r is influenced by several parameters, namely, the trapped charge, beam current, beam radius, material type, scanning potential and the working distance. Besides, there are additional factors that control the reflection point, namely, the radius of irradiated area and the penetration depth for the charged disc and multipole models, respectively.

3. RESULTS AND DISCUSSIONS

3.1 Surface potential

Clearly, the assumptions that lead to configuring the mathematical form of the charged disc and multipole model are not the same. A special rule was therefore followed in order to obtain an objective comparison between the surface potentials of these two models. However, the radius of the irradiated area (R_s) and so the penetration depth (r') are considered equivalent to each other throughout the comparison task. Indeed, some of the results presented in the literature [12, 19] are concerned in order to give practical relevance to the current procedure. Consequently, comparison calculations are performed regarding a trapped charge (Q_t) of amount 1.0 nC spread through a disc of radius $1.0 \mu\text{m}$ for a Poly Methyl Methacrylate (PMMA) sample, i.e. $\epsilon_r=2.6$. This means the same amount of Q_t accumulated within a $1.0 \mu\text{m}$ radius sphere of PMMA material as long as the multipole model is considered. It is worth to mention that this material has adopted to be a case study for all computations throughout this work.

The results of the Eq. (3) and Eq. (5) is then represented in Figure 1 for $R_s = r' = 1.0 \mu\text{m}$. Actually, the distribution of the surface potential for the disc and multipolar approximations are plotted along the optical axis interval $0 \leq z \leq W$. Furthermore, the working distance W is considered throughout this work to be set at the experimental value 15 mm. Apparently, Figure 1 shows that the distributions of the two considered models are identical in a practical sense. Actually, careful review of the data for this result reveals that the similarity between these two curves decreases close to the sample region. In other words, there is an excellent similarity between the surface potential distribution of the charged disc and multipole models in regions away from the sample surface. While this match progressively diminishes as long as the approach to the sample surface.

In addition, as the depth of penetration (and therefore the radius of the irradiated area) increases, the mismatches in a potential curve near the sample become more significant, see Figure 1(b). In fact, the inserts in Figure 1 have been added to further illustrate the above-mentioned result. Where the potential area is traced according to $1/z$ instead of z itself.

It worth to mention that the deviation in the similarity mainly comes from the curve of the multipole approximation rather than the charged disc. Actually, such behavior in the potential curve for multipole approximation clearly shows that, when the irradiated sample area increases, the influence of the higher terms becomes significant. In other words, the weight of multipole moments of higher order becomes significantly influencing the potential distribution as a wider

area is irradiated. Indeed, this is a reasonable consequence since a wider area of accumulated electrons proved a high degree of freedom for these charges to manifest themselves with dipole and octupole, see Eq. (5). Therefore, the point charge model offers distributions that almost similar to the two models considered in this work when R_s and r' decrease. In other words, the point charge approximation can efficiently use to simulate the surface potential for low irradiation potential and narrow irradiated area.

Accordingly, more attention needs to be paid to testing dielectric materials with high dielectric constants at higher accelerating potentials. Concerning the typical use of SEM, the coating of such a type of material should grant erasing its ability to trap the incident electrons. Hence, all the incident electrons should leak to the ground to avoid the charging effect. As far as the mirror mode operation for SEM is concerned, the type of material under consideration should be exactly isolated from the stage in order to get enhanced electron mirror images. Anyway, at low accelerating-test potential, the mentioned type of material and that with a lower dielectric constant need no caution in the examination process, whether the SEM is used in the usual or mirror mode.

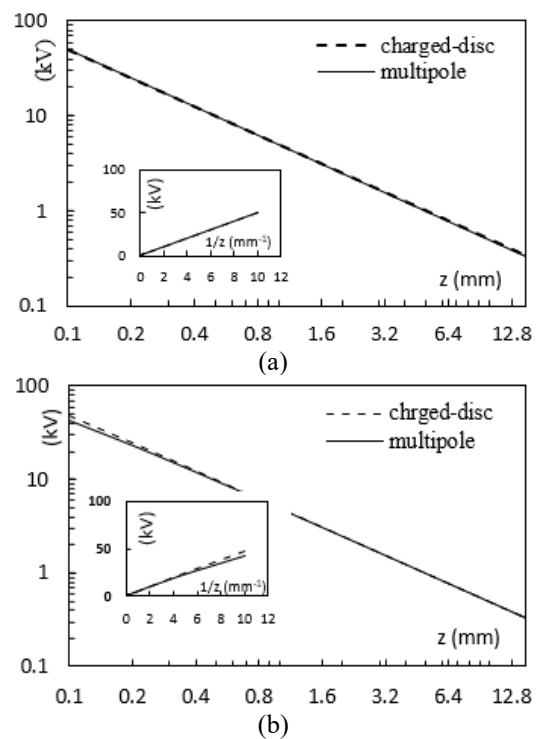


Figure 1. The distributions of surface potential of the charged disc and multipole models for (a) $R_s = r' = 1.0 \mu\text{m}$ and (b) $R_s = r' = 40.0 \mu\text{m}$

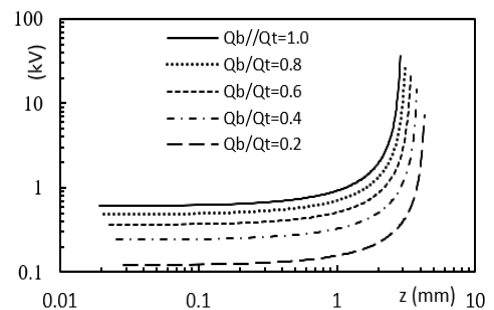


Figure 2. The distributions of beam surface potential for various values of the beam to trapped charge's quotient

3.2 Beam current

Calculations throughout this context are implemented for the following values of $Q_i=1.0$ nC, $R_s=R_b=0.3$ mm, $r'=4.0$ μ m and $V_{sc}=1.0$ kV. The deduced beam potential distribution along the optical axis z is plotted in Figure 2 for various values of the beam to trapped charge's quotient. Indeed, these curves represent the weights of the beam potential along the interval between the beam reflection point and the sample surface. Clearly, the curves show that the beam potential distribution has a maximum value located at the beam surface.

The reason behind the maximum value of the beam potential can directly understood from Eq. (2). Typically, such an equation has derived according to an aspect of Coulomb's law, which shows an inverse correlation between the field (potential) and the distance of the source-charge distribution. Strictly speaking, the influence strength decreases as the observer point location increases and vice versa. Figure 2 itself can provide evidence for this inclusion through the observation of the behavior of the curve maxima with a variation of the Q_b/Q_t quotient. Obviously, these maxima get lower values as long as they are being a reduction in the Q_b/Q_t quotient. In other words, whenever the beam current decreases, the potential strength also decreases as a direct consequence of Coulomb's law, as depicted in Figure 3. Therefore, the electron beam current may be used as a fine-tuning to get images of high quality in SEM. In other words, the user of SEM could use the controlling of the beam current, together with the scanning potential, to obtain fine images.

Another remark could be read from the Figure 2, that the values of maxima abruptly decrease as the distance from the beam surface increases. Indeed, such drops reach values less than ~ 1 kV for distances less than ~ 2 mm away from the beam surface. This result gives indication that the real interaction between the sample and beam potential significantly fulfils within such a range, beforehand the reflection point. Moreover, the reduction in maxima applies along the beam potential distribution by almost the same amount as long as the quotient Q_b/Q_t decreases. On the other hand, Figure 2 reveals that the diminutions in Q_b/Q_t quotient lead to an inability for the electron beam to approach from the sample. Definitely, this means that the reduction in the beam current leads to a lessening in the beam potential strength. Theorem, the beam reflection point becomes far away from the sample whenever the quotient Q_b/Q_t drops.

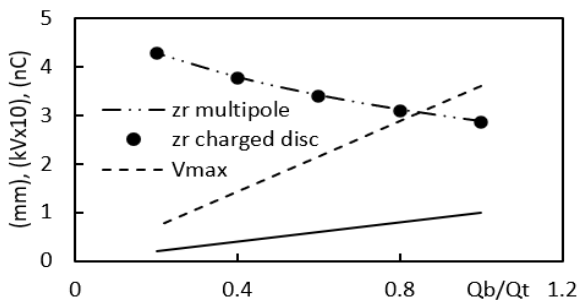


Figure 3. The reflection point, beam current and beam potential maxima for various values of the beam to trapped charge's quotient

The reflection points of the incident electron beam for the multipole and disc models at various values of Q_b/Q_t quotient are shown in Figure 3. It is seen that an excellent agreement between the curve of z_r that belongs to multipole and its

counterpart for disc models. As expected, the electron beam reflection moves toward the sample as the quotient Q_b/Q_t increased. Indeed, this result can be easily interpreted concerning of the beam current curve. Strictly speaking, the increment of Q_b/Q_t quotient, keeping Q_t fixed, leads to enlarge the beam current. This definitely means that the number of electrons, which synthesis the beam surface has augmented due the rise in Q_b . Therefore, the electron beam becomes able to penetrate much more through the field of sample potential. Hence, the incident electrons approach further from the sample because its driving potential has improved, see the curve of the maxima in Figure 3.

3.3 Scanning potential

Almost an SEM user depends mainly on the usage of scanning potential to be a principle adjusting parameter to obtain acceptable images. So, one may initially expect that such parameter is the supreme one that influences on the electron reflection point. However, the influence of this parameter has investigated throughout this context for the same values of Q_t , R_s , R_b and r' mentioned in the last section. Moreover, the values of scanning potential that are used for such enquiry are selected to be within the range $1 \geq V_{sc} \geq 40$ kV. It is worth to mention that SEMs typically operates with beam potential in the range $10 \geq V_{sc} \geq 30$ kV for normal usage. Nevertheless, as long as the mirror effect is concerned, the lower limit of V_{sc} usually reduces to 1.0 kV. Additionally, the using of scanning potential at about 40 kV is usually needed for some special applications; see for example, the literature [20].

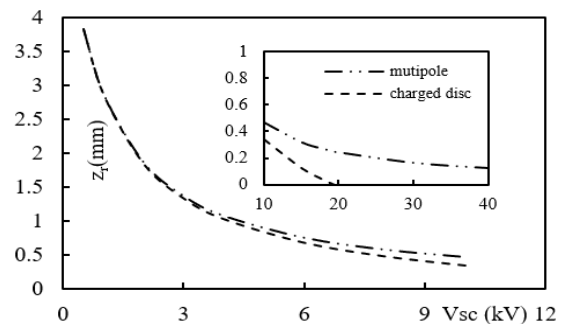


Figure 4. Variation of the reflection point versus scanning potential for multipole and disc approximations

Figure 4 reveals the variation of the incident-electron reflection point as a function of the scanning potential for the two considered models. Clearly, the use of a higher value of scanning potential leads the incoming electron to reflect closer to the sample. This is a logical consequence, indeed, since the adoption of a high driving potential confers to the incident electron an additional ability to go deeply into the active region of the surface potential. It is seen that both models expose a similar resistance against the incoming electrons for scanning potential less than ~ 3.0 kV. Where for both of them, the electron beam reflected back at a distance ~ 1.3 mm away from the sample surface. While the match between the two curves of z_r diminishes gradually beyond this value of V_{sc} . Strictly speaking, at higher accelerating potential, the surface potential of the multipole approximation shows a stronger resistance to the incident electrons than that of the disc approximation. Consequently, an incoming electron penetrates deeper towards the sample for the case of the disc

model in comparison with the multipole one.

In fact, an incident electron overcomes the surface potential resistance of the disc model and hits the sample surface when the accelerating potential reaches the value ~ 19.5 kV. While, the same incident electron at this potential approaches a distance about 0.25 mm away from the sample, for the case of the multipole model. In the same sense, this electron is still away from the sample surface by a distance ~ 0.1 mm, although it accelerated by 40 kV. Almost, such behavior is far from reality and the reason is the mathematical nature of multipole approximation, which prevents the assessment of potential on the surface. Such a mathematical formulation may record to be a disadvantage to the multipole model in comparison with the disc model.

Actually, this disadvantageous causes another undesirable consequence that the trapped charges can never be evaluated in terms of the maximum scanning potential. It is well known that such a potential may represent the maximum accelerating potential at which a stable mirror image could be observed without incident electrons hitting the sample. Therefore, the multipole model shares this detrimental with the charged point model. Practically, this unfavorable could be overcome by excluding areas that are so close to the sample.

3.4 Material type

Besides the PMMA material, several dielectric types were selected in order to explore the influence of the material's type on the surface potential and thus the corresponding response of the incident electron. These materials are Polymethylpentene (PMP), Polyphenylene sulfide (PPS), Polyethersulfone (PESU) and Polyoxymethylene (Acetal) impact modified (POM). The relative permittivity (ϵ_r) of these materials is respectively 2.1, 3.0, 3.5 and 4.0. Figure 5 shows the surface potential distributions of these materials along the working distance. Actually, these curves are deduced regarding $V_{sc}=10$ kV and the same values of Q_t , R_s , R_b and r' mentioned in the last section.

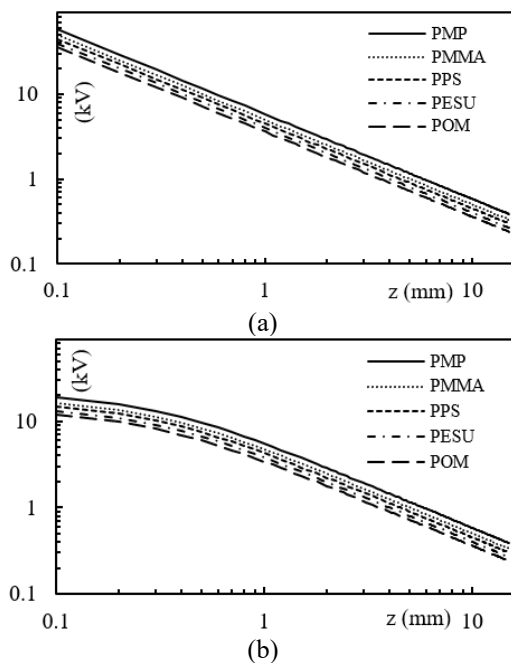


Figure 5. Distribution of the surface potential along the working distance of various polymers for (a) multipole and (b) charged-disc models

It is seen that the increment in the values of the dielectric constant leads to reduce the potential distribution by the same amount approximately along the working distance interval. This result can be thought directly from Eq. (3) and Eq. (5) since the potential expressions of both models are being divided by (ϵ_{r+1}) . Physically, however, the reduction of potential strength is due to increased permittivity. In other words, increases in ϵ_r mean an increase in the material's ability to store the electrostatic energy that results in a reduction in the potential outside the material. Therefore, it may be argued that as long as the trapped charges are accumulated in the material of high degree of polarization, the deduced potential becomes lower. Therefore, it may first realize that when a material with high permittivity is used to produce mirror effects, the incident electrons reflect closer to the sample surface, as shown in Figure 6. Indeed, it is a self-evident consequence since the surface potential annihilates with the growth of ϵ_r . Here also, one may detect the effect of the mathematical structure of potential on the behavior of the reflection point. Figure 6 clearly shows that the incoming electron slowly approaches the sample in the case of the charged disc model, whereas it is being abruptly for the multipole model.

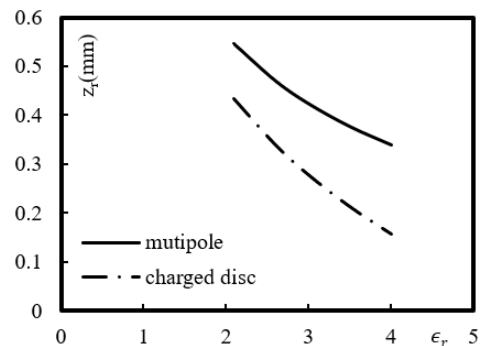


Figure 6. Variation of the reflection point versus permittivity for multipole and disc approximations

4. CONCLUSIONS

All in all, the results of this work have shown several important remarks concerning the preference of any of the two adopted models over its counterpart the other one. Indeed, the multipole model has features that can be regarded as controversial. Strictly speaking, although this model has many strengths compared to its peers, it has a number of weaknesses at the same time. The advantages of the multipole model have extensively discussed previously [16, 17]. Accordingly, the model of multipole is a powerful tool for detecting the real distribution of trapped charges within insulators. Furthermore, it may efficiently adopt to reveal how these charges arrange them self for such distribution.

Unfortunately, the results of the present work clearly shows that the multipole model has a critical disadvantageous due to its mathematical representation. Specifically, such a mathematical expression does not give the capability for computing the surface potential at the sample surface; moreover, the outcomes of this approximation at distances less than ~ 0.5 mm close the sample surface are almost inaccurate. In other words, the multipole model could never be used for estimating the trapped charges amount as in terms of so-called maximum scanning potential.

Nevertheless, the multipole model works well along distances about 97% of a working distance. Thus, such a relatively long distance, compared with the remaining one of the working distance, is sufficient to adopt the multipole model in the simulation of practical experiments. Keeping in mind that such a model is exceptional in detecting the trapped charge profile and the type of arrangements that these charges may take.

On the other hand, the multiple model seems excellent for simulating the surface potential that arises due to a higher number of localized short-range trapped charges. Conversely, the charged-disk model effectively approximates the surface potential that occurs due to a trapped charge spread within a relatively long range.

REFERENCES

[1] Liebault, J., Moya-Siesse, D., Bernardini, J., Moya, G. (2002). Charge trapping characterization in the thin oxide layer/non-conductive substrate system. *Surface and Interface Analysis*, 34(1): 668-671. <https://doi.org/10.1002/sia.1384>

[2] Touzin, M., Goeriot, D., Guerret-Piécourt, C., Juvé D., Tréheux D., Fitting H.J. (2006). Electron beam charging of insulators: A self-consistent flight-drift model. *Journal of Applied Physics*, 99(11): 114110. <https://doi.org/10.1063/1.2201851>

[3] Croccolo, F., Riccardi, C. (2008). Observation of the ion-mirror effect during microscopy of insulating materials. *Journal of Microscopy*, 229(1): 39-43. <https://doi.org/10.1111/j.1365-2818.2007.01866.x>

[4] Liebault, J., Zarbout, K., Moya, G., Kallel, A. (2003). Advanced measurement techniques of space-charge induced by an electron beam irradiation in thin dielectric layers. *Journal of Non-Crystalline Solids*, 322(1-3): 213-218. [https://doi.org/10.1016/S0022-3093\(03\)00204-7](https://doi.org/10.1016/S0022-3093(03)00204-7)

[5] Asokan T., Sudarshan T.S. (1994). Analysis of the scanning electron microscope mirror image based on the dielectric surface microstructure. *Journal of Applied Physics*, 75(8): 3715-3722. <https://doi.org/10.1063/1.356043>

[6] Wintle, H.J. (1999). Analysis of the scanning electron microscope mirror method for studying space charge in insulators. *Journal of Applied Physics*, 86(11): 5961-5967. <https://doi.org/10.1063/1.371640>

[7] Vallayer, B., Blaise, G., Treheux, D. (1999). Space charge measurement in a dielectric material after irradiation with a 30kV electron beam: Application to single crystals oxide trapping properties. *Review of Scientific Instruments*, 70(7): 3102-3112. <https://doi.org/10.1063/1.1149887>

[8] Al-Obaidi H.N., Khaleel I.H. (2013). Computational investigation of electron path inside SEM chamber in mirror effect phenomenon. *Micron*, 51: 13-20. <https://doi.org/10.1016/j.micron.2013.06.003>

[9] Al-Obaidi, H.N. (2015). Beam analysis of scanning electron microscope according to the mirror effect phenomenon. *Journal of Electrostatics*, 74: 102-107. <https://doi.org/10.1016/j.elstat.2015.01.004>

[10] Al-Obaidi, H.N., Abid, M.M., Kadhém W.J. (2016). Investigation of scanning electron beam parameters in terms of the disk-charged approximation for the sample potential. *Optik*, 127(17): 6978-6981.

<https://doi.org/10.1016/j.ijleo.2016.05.017>

[11] Coelho, R., Aladenize, B., Garros, B., Acroute, D., Mirebeau, P. (1999). Toward a quantitative analysis of the mirror method for characterizing insulation. *IEEE Transactions on Dielectrics and Electrical Insulation*, 6(2): 202-210. <https://doi.org/10.1109/94.765911>

[12] Chen, H., Gong, H., Ong, C.K. (1994). Classical electron trajectory in scanning electron microscope mirror image method. *Journal of Applied Physics*, 76(2): 806-809. <https://doi.org/10.1063/1.357753>

[13] Temga T., Guerret-Piécourt C., Juvé D., Tréheux D. (2002). Conduction and trapping mechanisms in monocrystalline titanium dioxide through the mirror method. In *Annual Report Conference on Electrical Insulation and Dielectric Phenomena*, Cancun, Mexico, pp. 656-659. <https://doi.org/10.1109/CEIDP.2002.1048881>

[14] Ghorbel, N., Kallel, A., Damamme, G., Renoud, R., Fakhfakh, Z. (2006). Analytical description of mirror plot in insulating target. *The European Physical Journal Applied Physics*, 36(3): 271-279. <https://doi.org/10.1051/epjap:2006130>

[15] Ghorbel, N., Kallel, A., Damamme, G. (2012). Modeling electric charge distribution on insulator under electron bombardment: Case of rectangular surface implantation. *AIP Advances*, 2(1): 012190. <https://doi.org/10.1063/1.3700435>

[16] Al-Obaidi, H.N., Mahdi, A.S., Khaleel, I.H. (2018). Characterization of trapped charges distribution in terms of mirror plot curve. *Ultramicroscopy*, 184: 12-18. <https://doi.org/10.1016/j.ultramic.2017.08.001>

[17] Mahdi, A.S., Al-Obaidi, H.N., Husien H.K. (2022). Investigation of trapped charges profile for an irradiated insulated material. *Journal of Microscopy*, 286(3): 245-251. <https://doi.org/10.1111/jmi.13103>

[18] Al-Obaidi, H.N., Mahdi, A.S., Khaleel, I.H. (2018). Characterization of trapped charges distribution in terms of mirror plot curve. *Ultramicroscopy*, 184: 12-16. <https://doi.org/10.1016/j.ultramic.2017.08.001>

[19] Chen, H., Gong, H., Ong, C.K. (1995). Determination of charge distribution volume in electron irradiated insulators by scanning electron microscope. *Journal of Applied Physics*, 78(6): 3714-3718. <https://doi.org/10.1063/1.359950>

[20] Kim, K.W. (2021). Some living eukaryotes during and after scanning electron microscopy. *Applied Microscopy*, 51(1): 16. <https://doi.org/10.1186/s42649-021-00065-8>

NOMENCLATURE

I_b	beam current, A
K	dimensionless constant
Q	amount of charges, C
Q_b	amount of electrons in a beam cross section area, C
Q_t	amount of trapped electrons, C
R	radius of a charged-disc of charges, m
R_b	radius of a charged-disc of electrons beam, m
R_s	radius of a charged-disc of trapped electrons, m
r	radius of spherical volume element, m
T	time, s
U	electric potential due to a charged-disc R , V
U_b	electric potential due to a charged-disc R_b , V

U_{sd}	electric potential due to a charged-disc R_s , V
U_{sm}	electric potential according to multipole model, V
W	working distance, m
z	vertical distance where potential is observed, m
z_r	electron reflection point, m

Greek symbols

ϵ_m	material permittivity, F.m ⁻¹
ϵ_o	space permittivity, F.m ⁻¹
ϵ_r	relative permittivity, F.m ⁻¹

ρ	radial point where U_{sm} is observed, m
--------	--

Subscripts

b	beam of electrons
sd	surface with charged-disc model
sm	surface with multipolar model
s	sample surface
t	trapped electrons
r	reflection